Structural correlations and phonon density of states in $GeSe_2$: A molecular-dynamics study of molten and amorphous states

P. Vashishta
*Laboratory of Atomic and Solid State Physics, Cornell University, Ithaca, New York 14853-2501 and Argonne National Laboratory, Argonne, Illinois 60439-4843**

Rajiv K. Kalia
Argonne National Laboratory, Argonne, Illinois 60439-4843

I. Ebbsjö
Studsvik Neutron Research Laboratory, S-611 82 Nyköping, Sweden
(Received 8 August 1988)

With use of the molecular-dynamics technique, the structural and dynamical correlations in molten and vitreous $GeSe_2$ are investigated with an effective interionic potential which consists of Coulomb, charge-dipole, and steric interactions. It is found that the short-range order is dominated by $Ge(Se_{1/2})_4$ tetrahedra and the Ge—Se, Se—Se, and Ge—Ge bond lengths are 2.35, 3.75, and 4.30 Å, respectively. The static-structure factor exhibits the first sharp diffraction peak (FSDP)—a characteristic of the intermediate-range order in binary chalcogenide glasses. Partial pair-distribution functions and the corresponding static-structure factors indicate that Ge correlations are responsible for the FSDP, which is in agreement with differential-anomalous-scattering experiments. In the vitreous state, the FSDP displays an anomalous variation with temperature in that its height increases while the other peaks decrease in height upon heating. All the other peaks observed in the structural measurements are also found present in the calculated static-structure factor. The peak positions and their relative heights in the liquid and glass compare favorably with experiments. The calculated phonon density of states in the glass shows peaks at 8.0, 10.8, 26.4, 34.4, and 37.2 meV, which are in good agreement with the positions of the main peaks in inelastic-neutron-scattering experiments. In addition, we find a companion line of the symmetric breathing mode A_1 (26.4 meV) at 27.8 meV. Raman-scattering experiments also find the companion line to be ~ 1.5 meV higher than the A_1 mode. The calculated phonon density of states has weaker features at 12.6, 17.2, and 22.0 meV and they are also observed by inelastic-neutron-scattering and Raman-scattering experiments.

I. INTRODUCTION

In recent years there have been several neutron- and x-ray-scattering studies[1–4] of the structural properties of molten and vitreous $GeSe_2$. These studies show that the molten and glassy states are structurally similar and the peaks (except the first one) in the static-structure factor sharpen on cooling. In chalcogenide glasses a great deal of attention has been paid to the first sharp diffraction peak (FSDP).[5–14] The explanations for the origin of this peak range from layerlike correlations[7] to random packing of structural units.[5] Theoretical attempts have not yet been made to investigate the structural properties of molten and glassy $GeSe_2$.

There are several experimental[15–31] and theoretical[32–34] studies of the vibrational properties of Ge-Se system. Recent inelastic-neutron-scattering measurements of phonon density of states by Walter, Price, Susman, and Volin[15] reveal five peaks between 9 and 37 meV. At the corresponding energies, Raman-active lines have also been observed.[21] Four of these peaks can be identified with the vibrational modes of an isolated tetrahedron of $Ge(Se_{1/2})_4$. Sen and Thorpe[34] have proposed a model in which they attempt to explain the vibrational states of AB_2-type glasses in terms of the $A—B—A$ bond angle: If the bond angle is much below the critical value θ_c (136° in $GeSe_2$), it is argued that the frequency spectrum is due to vibrational states of weakly coupled AB_4 tetrahedral units whereas for $\theta > \theta_c$ the spectrum is dominated by bandlike modes. It is further suggested that the Ge—Se—Ge bond angle is around 90° and therefore the vibrational frequency should be dominated by molecular tetrahedral units of $Ge(Se_{1/2})_4$.

This paper deals with the structural properties of molten and amorphous $GeSe_2$, and the phonon spectrum of the glass. These properties are investigated with use of the molecular-dynamics simulation with an effective interionic potential. The scheme for constructing the potential is general enough to address SiO_2, GeO_2, and the whole series of binary chalcogenides. The basic ingredients of the model potential are steric repulsions, long-range Coulomb potentials, and charge-dipole interactions among the constituent ions. Using this potential molecular-dynamics calculations are carried out in the molten and glassy states of 648- and 5184-particle systems with periodic boundary conditions. The structural information for the system is obtained from partial pair-

distribution functions, static-structure factors, bond-angle distributions, and rings. Our results for the static-structure factor show all the peaks observed in neutron[3]- and x-ray[1]-scattering measurements. The positions of these peaks and their relative heights are in good agreement with experimental results. The results for bond lengths, coordination numbers, and bond-angle distributions reveal that the system consists of slightly distorted $Ge(Se_{1/2})_4$ tetrahedra in the amorphous and molten states. The bond lengths of Ge—Se and Se—Se are found to be 2.35 and 3.75 Å, respectively, which are in good agreement with structural measurements.[1–4] The Ge—Ge nearest-neighbor distance is found to be 4.3 Å. Our structural results also shed light on the arrangement of $Ge(Se_{1/2})_4$ tetrahedral units, vis-a-vis, corner-sharing and/or edge sharing. From the analysis of twofold rings we determine that 5% of the tetrahedra are edge sharing and that the remaining tetrahedra share corners. We observe the well-known first sharp diffraction peak in the static-structure factor of both molten and glassy states. From partial pair-distribution functions, we find that the FSDP is primarily due to Ge-Ge and Ge-Se correlations. Differential-anomalous-scattering experiments[35] indicate that Ge correlations are in fact responsible for the FSDP. The FSDP also displays its characteristic anomalous temperature dependence[1]—a feature common to SiO_2, As_2Se_3, and many other binary chalcogenide glasses.[8–11]

We have also calculated the frequency spectra of velocity and position autocorrelation functions. At low temperatures these spectra relate to the phonon density of states. In the amorphous state the density of states shows the five prominent peaks observed by Walter *et al.*[15] in the inelastic-neutron-scattering measurements. The peaks occur at 8.0, 10.8, 26.4, 34.4, and 37.2 meV, all very close to the experimental values. The peak at 26.4 meV corresponds to the well-known symmetric breathing mode A_1 and we also find a feature at 27.8 meV which we identify as the celebrated companion line[16,17,21] A_{1c} of A_1. The molecular-dynamics (MD) density of states also shows weaker features at 12.6, 17.2, and 22.0 meV. The first feature has been observed in neutron-scattering experiments[15] while a Raman-active line[21] has been found at 22 meV. The overall agreement with the experimental structure factor and phonon density of states gives confidence in the effective potential for a-$GeSe_2$.

The outline of this paper is as follows: In Sec. II we describe the effective potential for a-$GeSe_2$ and the details of the MD calculation are given in Sec. III. Starting with a brief discussion of the properties of molten $GeSe_2$ in Sec. III A, we sketch in Sec. III B how the vitreous states are obtained by quenching the molten states. Section IV is subdivided into MD results for structural correlations and the phonon density of states. Using the partial and total pair-correlation functions, the corresponding static-structure factors and the various bond-angle distributions, we first discuss the short- and the intermediate-range orders. This is followed by a discussion of the displacement and velocity autocorrelation functions, their frequency spectra, and the phonon density of states. Section V presents a critique of the present work.

II. INTERACTION POTENTIAL

Three-body forces are essential in the cohesion of elemental semiconductors. For instance, a diamond lattice is unstable against a closed-packed structure with just central interatomic forces. However, binary systems like $GeSe_2$ and SiO_2 are different in that the cohesion arises from the shortest bond, namely, the Ge—Se bond. This involves a charge transfer from Ge to Se (or Si to O), which imparts an ionic character to them. The negative ions O^{2-} or Se^{2-} are large and consequently have large electronic polarizabilities, which leads to a very substantial charge-dipole interaction. Thus, the effective potential for $GeSe_2$ or SiO_2-type systems should have at least three ingredients: the Coulomb and charge-dipole interactions, and a steric repulsion to balance them.[36–38] In $GeSe_2$ and SiO_2 three-body forces may be important but, ignoring this for the time being, our aim at first is to investigate systematically the properties of $GeSe_2$, and subsequently $SiSe_2$, SiO_2, GeO_2 and other chalcogenide glasses using an effective two-body potential in molecular-dynamics calculations.[38] The intent is to use the same functional form of the potential for all of these systems and then through a detailed comparison with structural and phonon density-of-states measurements, we expect to gain insight into the successful features and, more importantly, into the limitations of central-force models. This may provide a reasonable prescription for three-body forces in binary semiconducting glasses.

In the effective potential we have constructed, Ge and Se are treated as ions having effective charges of $+4Z$ and $-2Z$, respectively. These charges give rise to the Coulomb interaction and a charge-dipole potential since the larger ions are highly polarizable. The effective interaction also includes steric repulsion among Ge and Se ions. The total interparticle potential is of the form

$$\phi_{ij}(r)=\frac{Z_iZ_j}{r}-\frac{\frac{1}{2}(\alpha_iZ_j^2+\alpha_jZ_i^2)}{r^4}e^{-r/r_{4s}}+A_{ij}\left[\frac{\sigma_i+\sigma_j}{r}\right]^{\eta_{ij}}, \quad (1)$$

where Z_i, σ_i, and α_i denote the effective charge, radius and polarizability of the ith ion. Since the size of Ge^{4+} is much smaller than that of Se^{2-}, we neglect the polarizability of the Ge^{4+} ion. The electronic polarizability of Se^{2-} is in the range of 7–10.5 $Å^3$ and the value we have taken is on the lower end of this range.[39] The exponential screening term in the charge-dipole interaction provides a reasonable cutoff for the r^{-4} interaction. Taking the decay length, r_{4s}, to be 4.43 Å, the charge-dipole potential at the edge ($L/2$) of the cell of the smaller ($N=648$) MD system is reduced to 4% of the charge-dipole potential without the exponential term.

In a binary system there are three distinct coefficients A_{ij} and exponents η_{ij}. If the cohesive energy, bulk modulus, and the elastic constants were reliably known in the low-temperature crystalline phase, these could be used to determine A and the three exponents η_{ij}. For simplicity we have taken all three A's to be the same, but different exponents are chosen for Ge-Ge, Ge-Se, and Se-

Se. The optimum choice for $\eta_{\text{Ge-Ge}}$, $\eta_{\text{Ge-Se}}$, and $\eta_{\text{Se-Se}}$ is found to be 11, 9, and 7, respectively.[37] Since the charge on Ge is $+4Z$ and its size is small, the Coulomb repulsion is dominant and the steric Ge-Ge repulsion is negligible. The value of A is chosen to give a slightly positive pressure in the liquid phase. This leaves the determination of Z, σ_{Ge}, and σ_{Se}. The latter two are taken to be 0.73 and 2.0 Å. In the present scheme the sum of σ_{Ge} and σ_{Se} does not give the Ge—Se bond length, but it is the total interaction potential that determines the bond lengths. The only remaining parameter, Z, is determined from the melting temperature and the optimum value of Z is found to be $0.33e$. With these parameters the melting temperature is estimated to be 1020±20 K, which is close to the experimental value.[40] The parameters of the effective potential are listed in Table I and $\phi_{\text{Ge-Ge}}(r)$, $\phi_{\text{Ge-Se}}(r)$, and $\phi_{\text{Se-Se}}(r)$ are shown in Fig. 1.

III. CALCULATIONS

Molecular-dynamics calculations are carried out in a (N,V,E) ensemble of $N=648$ (216 Ge and 432 Se) particles in a cubic cell of volume L^3 with periodic boundary conditions. For the molten phase L is chosen to be 27.51 Å so that the number density corresponds to the experimental value,[41] 3.114×10^{22} cm^{-3}. The MD calculations for the amorphous state are performed in a cubic cell of edge 26.60 Å to give a density[41] of 3.443×10^{22} cm^{-3}. To estimate finite-size effects, molecular-dynamics calculations are also performed on a 5184-particle system. The edge of the corresponding MD cell is 55.02 Å in the molten state and 53.20 Å in the glass. The long-range nature of the Coulomb interaction is taken into account by Ewald's summation. The Newtonian equations of motion are integrated by Beeman's method[42] using a time step, $\Delta t=5\times10^{-15}$ s, which conserves the energy to better than 1 part in 10^4 over several thousand time steps.

A. Characterization of molten states

The calculations are started at a density of 3.443×10^{22} cm^{-3} with Ge and Se atoms residing on a cubic lattice. This system is heated to 1100 K and equilibrated for 15 000 time steps. At this stage the density of the system is lowered to the experimental value (3.114×10^{22} cm^{-3}) by appropriately scaling the positions of all the particles and the edge of the cubic MD cell to 27.51 Å. The resulting system is again equilibrated at 1100 K for 15 000 time steps. To remove any trace of the effect of initial conditions, the system is further heated to 2000 K and thermalized for 18 000 time steps. This high-temperature liquid has no memory of the initial conditions. The molten state at 2000 K is cooled to 1500 K and equilibrated for several thousand time steps. The resulting system is further cooled and equilibrated at 1100 K. Thermal averages of each system are calculated over 36 000 time steps.

Figure 2 shows the temperature dependence of the internal energy and the constants of self-diffusion for Ge and Se in the molten states. It is clear that the diffusion is relatively small in the molten state at 1100 K. When the low-temperature system is heated gradually, the onset of diffusion is observed around 1100 K which indicates that the melting temperature is somewhat less than 1100 K. The experimental value[40] is close to 1000 K. Although we have not yet investigated the melting transition for the 5184-particle system, we expect the transition region to be narrower than that for the 648-particle system.

B. Preparation of vitreous states

The molten state at 1100 K is quenched by reducing the velocity of each particle by 0.1% at intervals of 50 time steps. The rate of quenching and the intermediate relaxation time are adjusted so that one obtains a system at $T\approx600$ K ($T>T_m/2$) in which there is sufficient thermal energy for structural relaxation to lower-energy configurations. After quenching to approximately 600 K, the volume of the MD cell is decreased so that the number density corresponds to 3.443×10^{22} cm^{-3} and the system is thermalized for 15 000 time steps. In this way we obtain glassy states at 625 and 283 K. We have also done

TABLE I. Parameters of the effective potential for $GeSe_2$, Eq. (1).

Z	$0.33\|e\|$
A	249.7 meV
$\sigma_{Ge^{4+}}$	0.73 Å
$\sigma_{Se^{2-}}$	2.00 Å
η_{GeGe}	11
η_{GeSe}	9
η_{SeSe}	7
$Z_{Ge^{4+}}$	$1.32\|e\|$
$Z_{Se^{2-}}$	$-0.66\|e\|$
$\alpha_{Ge^{4+}}$	0
$\alpha_{Se^{2-}}$	7.0 Å^3
r_{4s}	4.43 Å

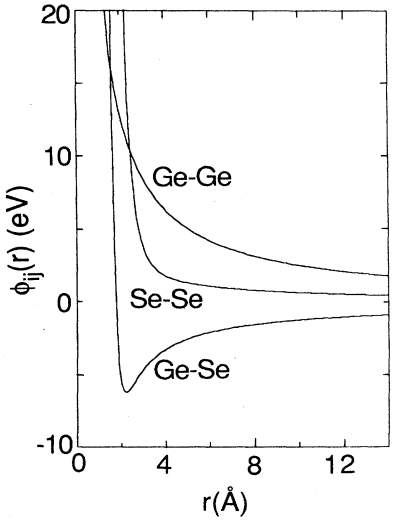

FIG. 1. Ge-Ge, Ge-Se, and Se-Se effective potentials in $GeSe_2$.

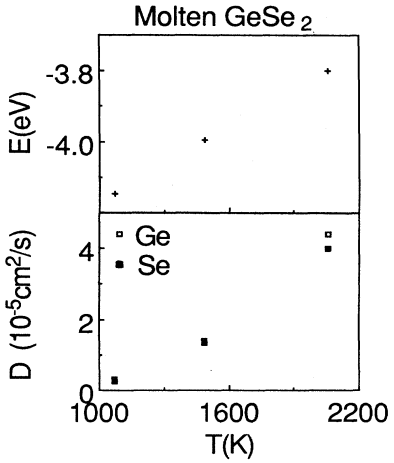

FIG. 2. Temperature variations of the energy per particle and the constants of self-diffusion for Ge and Se in the molten phase.

calculations where we first increase the density in the molten state at 1100 K and then quench the system to form vitreous states at 600 and 300 K. Because the cooling is done "slowly" over 30 000 time steps and the system is allowed to relax over a long period of time (36 000 time steps), the structural and vibrational properties are insensitive to whether the system is quenched first and then increased in density or vice versa. In each glass thermal averages are taken over 36 000 time steps.

IV. RESULTS

The foremost requirement of a computer simulation is that it provides a reasonable description of the structural properties, namely, the short- and medium-range order. In a-$GeSe_2$ the short-range order is dominated by $Ge(Se_{1/2})_4$ tetrahedral units and as we shall see momentarily, the MD results for bond lengths, nearest-neighbor coordinations, and bond-angle distributions confirm that these tetrahedra are present in the molten and vitreous states. The partial pair-distribution functions and bond-angle distributions also shed light on how the tetrahedra are connected (corner sharing and/or edge sharing) in space over medium-range order. There are several experimental studies of the structural properties of a-$GeSe_2$—by differential anomalous x-ray scattering, and also by x-ray-diffraction and neutron-diffraction techniques. There also exist exhaustive Raman-scattering and inelastic-neutron-scattering measurements on the vibrational spectrum of a-$GeSe_2$. These experiments on structural and vibrational properties provide a stringent test for computer simulations.

A. Structural properties

The results for partial pair-distribution functions, bond-angle distributions, and static-structure factors provide a complete picture of the short-range and intermediate-range orders.

1. Local order

The primary information about structural correlations is derived from partial pair-distribution functions $g_{\alpha\beta}(r)$. In a binary system these are defined by

$$\langle n_{\alpha\beta}(r)\rangle dr = 4\pi r^2 dr\, \rho C_\beta g_{\alpha\beta}(r) , \tag{2}$$

where $n_{\alpha\beta}(r)dr$ denotes the number of particles of species β around a particle of species α between shells of radii r and $r+dr$. ρ is the total number density and C_β is the concentration of species β. The brackets $\langle\ \rangle$ denote the thermal average as well as the average over all particles of species α.

Figures 3 and 4 show the partial pair-distribution functions in the molten and vitreous states, respectively. The total pair-distribution function in these states is displayed in Fig. 5. The pair-distribution functions for the molten and vitreous states are quite similar. In the glass the Ge—Se and Se—Se bond lengths, given by the positions of the first peaks in $g_{Ge—Se}$ and $g_{Se—Se}$, are found to be 2.35±0.05 Å and 3.75±0.05 Å, respectively. The corresponding distances are slightly larger (2.36 and 3.80 Å) in the molten state because the number density in the liquid is lower than in the glass. Experimental values for these quantities are 2.37 and 3.80 Å in the glass.[1–4]

In order to further determine the short-range correlations, it is essential to supplement the information on bond lengths with nearest-neighbor (NN) coordination

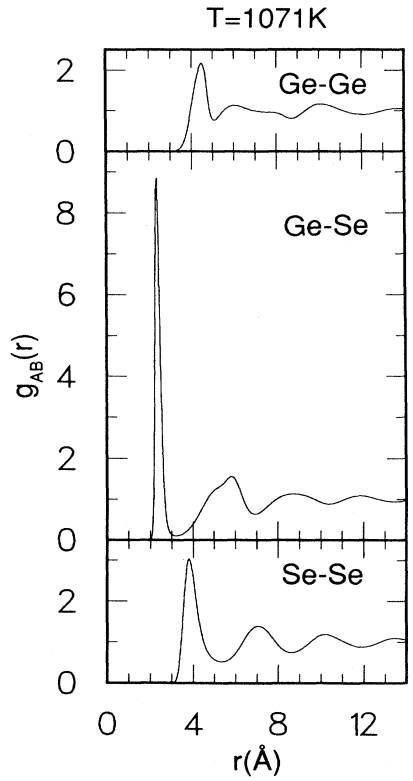

FIG. 3. Pair-distribution functions of Ge-Ge, Ge-Se, and Se-Se in molten $GeSe_2$ ($\rho = 3.114\times10^{22}$ cm^{-3}) at $T = 1071$ K.

numbers and bond angles. The coordination number $N_{\alpha\beta}(R)$ is obtained from,

$$N_{\alpha\beta}(R)=4\pi\rho C_\beta \int_0^R r^2 g_{\alpha\beta}(r)dr \ . \quad (3)$$

The NN coordination numbers of Ge and Se are found to be 4 and 2, respectively, in accordance with the $8-n$ rule.

The determination of short-range order requires not just the knowledge of partial pair-distribution functions but also the bond-angle distributions. The latter are obtained from the MD trajectories as follows: For B—A—B bond angles we first find the NN shell of A atoms from the distance at which the first peak in $g_{AB}(r)$ terminates. From the positions of the B atoms within the nearest-neighbor shell, a histogram of B-A-B angles is determined for all A atoms in each configuration. In the case of A-A-B distributions, the nearest-neighbor shells are taken to be the distances at which the first peaks in $g_{AA}(r)$ and $g_{AB}(r)$ terminate. The averages are taken over 100 configurations with successive configurations separated by 100 time steps. Each configuration is obtained by subjecting an MD trajectory to a steepest-descent quench[43] so that the velocity and force on each particle is zero. Figures 6 and 7 illustrate various bond-angle distributions in the liquid and glassy states, respectively. Thermal effects make these distributions considerably broader in the molten state. Also there are additional features in the glass, like the split peak around 120° in the Ge-Se-Ge distribution.

The Se-Ge-Se distribution exhibits a peak around 106°

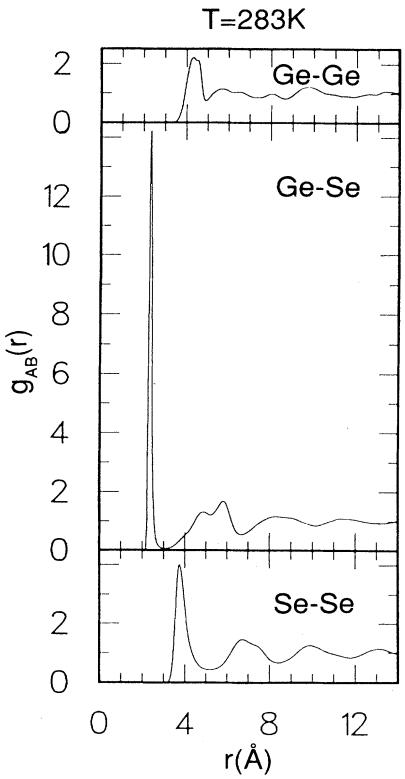

FIG. 4. Pair-distribution functions in a-$GeSe_2$ ($\rho=3.443\times10^{22}$ cm^{-3}) at $T=283$ K.

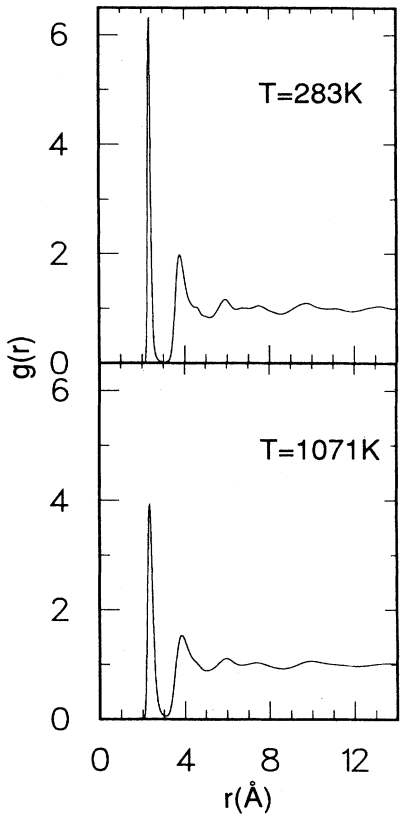

FIG. 5. Total pair-distribution functions of vitreous ($T=283$ K) and molten ($T=1071$ K) states.

while the Se-Se-Se and Ge-Se-Se distributions peak around 57° and 37°, respectively. The fact that each Ge is surrounded by four Se atoms with a 106° Se-Ge-Se angle and a 57° Se-Se-Se internal angle suggests the presence of slightly distorted $Ge(Se_{1/2})_4$ tetrahedra in the molten and vitreous states. For a perfect tetrahedron these angles

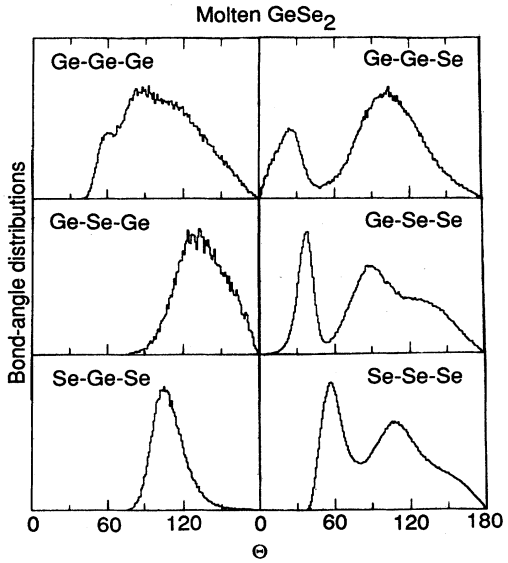

FIG. 6. Bond-angle distributions in molten $GeSe_2$ at $T=1071$ K.

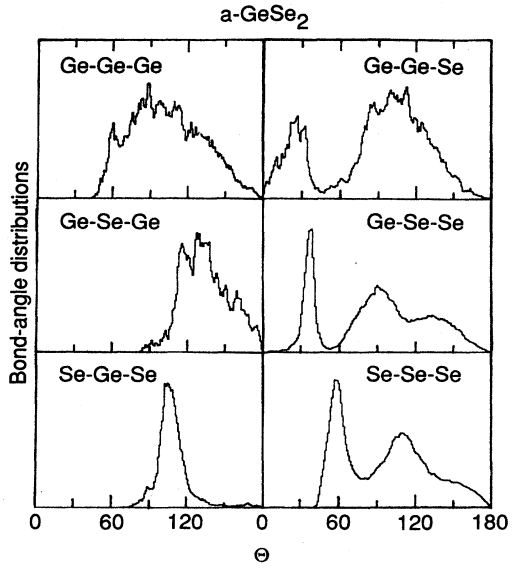

FIG. 7. Bond-angle distributions in a-$GeSe_2$ at $T=0$ K.

are 109.5°, 60°, and 35.3°. Note that the tetrahedra are not perfect even in the crystalline phase.[44] For example, Se-Ge-Se distribution has a sizeable width which is a reflection on the distribution of Se-Se distances.

Let us now focus on Ge-Ge correlations: From the first peak in the Ge-Ge pair-distribution function, one finds that each Ge has five nearest neighbors. On closer examination (Fig. 4) one can discern two peaks, one at 4.30 Å and the other at 4.50 Å, with coordinations of 3 and 2, respectively. In c-$GeSe_2$ the nearest-neighbor Ge-Ge separation in corner-sharing tetrahedra is 3.6 Å, and although the $Ge(Se_{1/2})_4$ tetrahedral units are common to the crystalline and glassy states, the packing of tetrahedra is expected to be quite different in the two phases. In the glass the nearest-neighbor Se-Se separation is 3.75 Å and the volume occupied by Se atoms $N_{Se}(4\pi/3)(1.88)^3$ $Å^3$ is 0.639 times the total volume of the MD cell. This volume fraction is very close to the random close-packing fraction for spheres (0.637). Thus the Se atoms occupy most of the available volume since the volume occupied by Ge atoms is negligible. The total number density and the volume fraction of Se atoms are expected to be larger in the crystalline phase than in the glass. Therefore, the nearest-neighbor separation between Ge atoms must be larger in the glass than in the crystal.

2. *Corner-sharing tetrahedra*

Medium-range correlations are determined by how $Ge(Se_{1/2})_4$ tetrahedra are connected to one another. Let us first consider two adjacent tetrahedra joined at a corner as shown in Fig. 8. The Ge atoms in the two tetrahedra are denoted by Ge_a and Ge_b. The Se atom common to the two tetrahedra Se_0 is chosen as the origin. The remaining Se atoms in the lower tetrahedron are labeled as Se_1, Se_2, and Se_3 whereas those in the upper tetrahedron are denoted by Se_4, Se_5, and Se_6. The z axis is along the line joining Ge_a and Se_0, and Se_1 and Se_4 are in the x-z plane of our frame of reference.

On the basis of the position of the second peak in the Ge-Se-Se distribution in Fig. 7, we take the angle between Ge_a—Se_0 and Se_0—Se_4 bonds to be 95°. Using the calculated Ge—Se (2.35 Å) and Se—Se (3.75 Å) bond lengths, one finds from Fig. 8 that Ge_a has a Se second neighbor (Se_4) at 4.6 Å and two more Se atoms as third neighbors (Se_5 and Se^6) at 5.7 Å. These relate to the observed peak around 5.8 Å and the shoulder near 4.8 Å in the Ge—Se pair-distribution function in Fig. 4. Figure 3 attests that this also holds in the molten phase. From the separations between Ge_a-Se_5 and Ge_a-Se_6, we determine the bond angles Ge_a—Se_0—Se_5 and Ge_a—Se_0—Se_6 to be 137°, which is consistent with the third peak at 140° in the Ge-Se-Se distribution in Fig. 7.

In Fig. 8 the distances are Se_2-Se_4=6.2 Å, Se_2-Se_5=7.5 Å, Se_2-Se_6=6.5 Å, and Se_1-Se_5=Se_1-Se_6=6.2 Å, etc. These distances give rise to a broad second peak around 6.7 Å in the Se-Se pair-distribution function, see Fig. 4. In Fig. 8 the Ge—Se—Ge bond angle is 130° and the Ge_a—Ge_b distance is 4.3 Å. The most prominent peak in the Ge—Se—Ge bond-angle distribution (Fig. 7) is around 125° and the first peak in the Ge-Ge pair-distribution function (Fig. 4) is at 4.3 Å. Thus, the corner-sharing tetrahedra connected as shown in Fig. 8 give rise to peaks that are consistent with the partial pair-distribution functions and the distribution of bond angles. For corner-sharing tetrahedra other possible connections can be ruled out because they cannot produce all of the significant features found in the partial pair-distribution functions and bond-angle distributions.

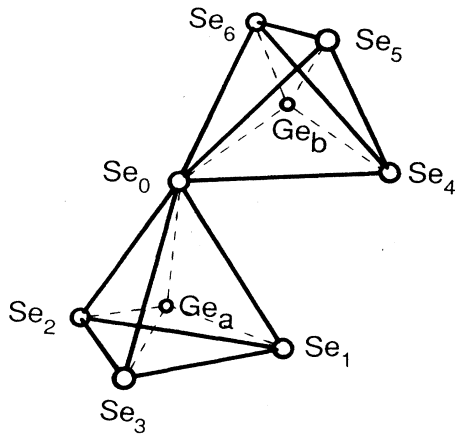

FIG. 8. Corner-sharing tetrahedra in a-$GeSe_2$. On the basis of the second peak in Ge-Se-Se distribution, the angle Ge_a-Se_0-Se_4 is taken to be 95°. The positions of all the atoms (in Å) are as follows: Se_0=(0,0,0), Ge_a=(0,0,−2.296), Se_1=(2.165,0,−3.062), Se_2=(−1.083,1.875,−3.062), Se_3=(−1.083,−1.875,−3.062), Ge_b=(1.752,0,1.484), Se_4=(3.736,0,0.327), Se_5=(1.637,−1.875,2.805), and Se_6=(1.637,1.875,2.805).

3. Edge-sharing tetrahedra

The bond-angle distributions indicate that a majority of tetrahedra share corners. However, in Ge—Se—Ge bond-angle distribution (Fig. 7) the tiny hump close to 90° arises from edge-sharing tetrahedra. Comparing the relative heights of the peaks around 90° and 125°, one finds that approximately 5% of the tetrahedra are edge bonded.

A more reliable estimate of the number of edge-sharing $Ge(Se_{1/2})_4$ tetrahedra can be obtained by counting the number of twofold rings or edge-sharing tetrahedra in the system. A typical twofold ring is shown in Fig. 9. To identity twofold rings we start with a Ge atom and treat it as the origin of the system. Within a radius of 3.0 Å which corresponds to the termination point of the first peak in $g_{\text{Ge-Se}}(r)$, we locate the nearest neighbors of the central Ge atom (Ge_a). On the average we expect to find four Se atoms (Se_1,Se_2,Se_3,Se_4) that constitute the corners of a tetrahedron around the Ge_a atom. Each Se on the average has two Ge nearest neighbors. Moving to one of the neighboring seleniums (Se_1) of Ge_a, we locate the other Ge nearest neighbor (Ge_b) of Se_1. From the second Ge atom (Ge_b) we proceed to one of its nearest neighbors (Se_2,Se_5,Se_6) excluding the previous one (Se_1). From the new Se position we determine if Ge_a is its nearest neighbor. This procedure is repeated for every Ge atom in a given glass configuration and we consider 100 configurations at intervals of $100\Delta t$ after performing the steepest-descent quench. In the case of the 648-particle system we find an average of 12 such rings in each configuration, which implies that 12 out of 216 tetrahedra share edges and the remaining tetrahedra are connected at the corners. Thus, approximately 5% of the tetrahedra share edges. Assuming 15% edge-sharing tetrahedra in a random-network model, Sugai[45] attempts to explain the intensity ratios of the symmetric-breaking mode and the companion line observed in the Raman spectrum. Our calculations for the phonon density of states in Sec. IV B show that the companion line (A_{1c}) arises from the vibrations of the tetrahedra belonging to fivefold and sevenfold rings. We expect that the inclusion of three-body forces in molecular-dynamics calculations will increase the number of edge-bonded tetrahedra.

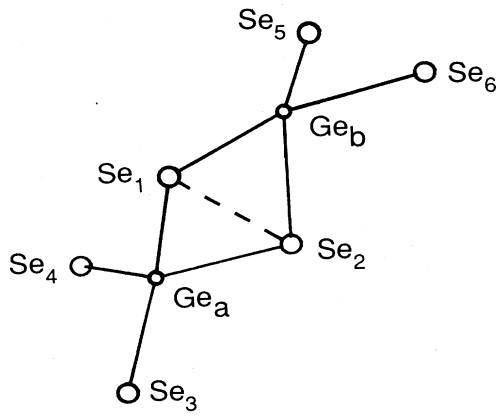

FIG. 9. A schematic of edge-sharing tetrahedra.

4. Static structure factor

The partial static-structure factors are obtained from the Fourier transforms of the corresponding pair-distribution functions:

$$S_{\alpha\beta}(q)=\delta_{\alpha\beta}+4\pi\rho(C_\alpha C_\beta)^{1/2}\int_0^\infty r^2[g_{\alpha\beta}(r)-1]\times\frac{\sin(qr)}{qr}dr\ . \tag{4}$$

The results in the molten and vitreous states are shown in Figs. 10 and 11. Thermal effects tend to broaden the peaks and in the high-temperature molten state ($T\approx 2000$ K) the first peak in $Se_{\text{Ge-Ge}}(q)$ is not clearly discernible.

To investigate the origin of various peaks in the partial static-structure factors, let us examine $g_{\alpha\beta}(r)$ and the remaining integrand in Eq. (4). The latter $[r^2\sin(qr)/qr]$ has maxima at $qr=2.03$, 7.98, 14.21, etc., and minima at 4.91, 11.09, etc. In $g_{\text{Ge-Se}}(r)$ the peak at 2.35 Å gives rise to a minimum in $S_{\text{Ge-Se}}(q)$ at $q=4.91/2.35\sim 2.1$ Å^{-1} and a maximum at $q=7.98/2.35\sim 3.4$ Å^{-1}. The peak at 5.8 Å contributes to the peak at $q=7.98/5.8\sim 1.4$ Å^{-1}. Similarly, the first peak in $g_{\text{Ge-Ge}}(r)$ at 4.3 Å gives rise to a peak near 1.9 Å in $S_{\text{Ge-Ge}}(q)$ and the first peak in the Se-Se partial structure factor is due to the peak at 3.75 Å in $g_{\text{Se-Se}}(r)$. For a quantitative understanding of the relationship between the peaks in the real and reciprocal spaces, the higher Fourier harmonics should be included.

The partial structure factors are combined according to

$$S_n(q)=\frac{\sum_{\alpha\beta} b_\alpha b_\beta (C_\alpha C_\beta)^{1/2}[S_{\alpha\beta}(q)-\delta_{\alpha\beta}+(C_\alpha C_\beta)^{1/2}]}{\left[\sum_\alpha C_\alpha b_\alpha\right]^2}\ , \tag{5}$$

to obtain the total structure factor for comparison with neutron-scattering measurements. In the above equations, C_α and b_α are the concentration and the coherent scattering length for the αth species. For Ge and Se the scattering lengths are 0.819×10^{-12} and 0.797×10^{-12} cm, respectively.[3] Figures 12 and 13 display the MD results for the neutron-static-structure factor in the molten and amorphous states, respectively. The open squares are the neutron-scattering measurements of Susman *et al.*[3] at 1084 and 10 K. The prominent features in the two figures are the peaks at 1.4, 2.0, 3.5, 5.6, and 8.7 Å^{-1}. In the glass there is an additional feature around 6.5 Å^{-1}. From partial static-structure factors, it is clear that the peak in $S_n(q)$ at 2.0 Å^{-1} is due to Se-Se correlations and the largest peak at 3.5 Å^{-1} is a result of all three correlations.

The MD results for peak positions compare very well with x-ray-diffraction[1] and neutron-diffraction[3] measurements. The relative heights of the peaks are also consistent with the experimental results. The only discrepancy is in the position of the first sharp diffraction peak: In MD simulations the peak is located between 1.3 and

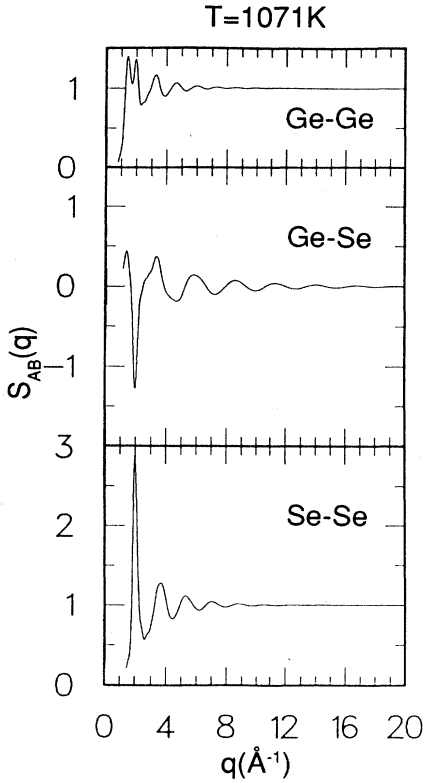

FIG. 10. Static-structure factors for Ge-Ge, Ge-Se, and Se-Se in molten GeSe at $T=1071$ K.

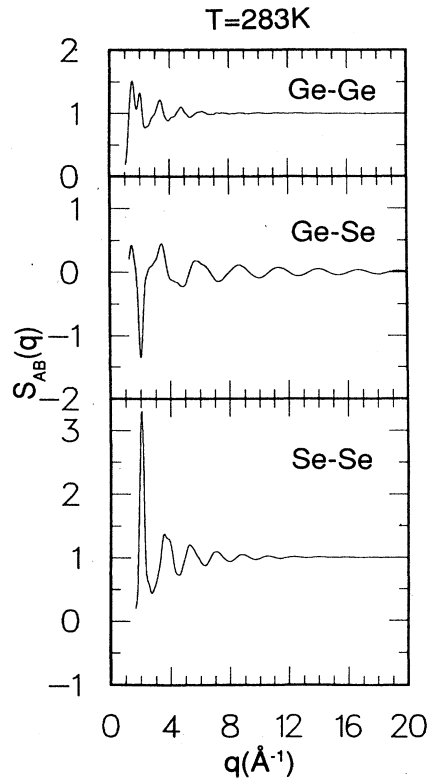

FIG. 11. Partial static-structure factors in a-$GeSe_2$ at $T=283$ K.

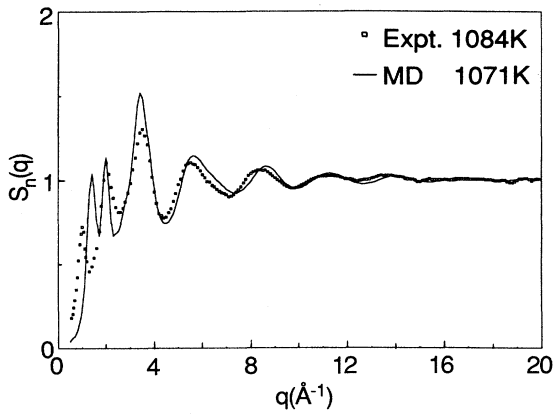

FIG. 12. Neutron-scattering static-structure factor in molten $GeSe_2$. Solid line, MD result at $T=1071$ K; open squares, experimental neutron-diffraction results at $T=1084$ K, Susman *et al.* (Ref. 15).

1.4 Å^{-1} whereas the experimental value is 1 Å^{-1}. This peak is the subject of a more detailed analysis in the next section.

5. *First sharp diffraction peak (FSDP)*

A sharp diffraction peak between 1.0 and 1.5 Å^{-1} is a feature common to SiO_2 and many binary chalcogenide glasses. In some systems the peak persists even in the molten state. An apparent oddity about the FSDP is that its height increases with an increase in temperature.[8–11] This anomalous behavior is reversible and occurs over a wide range of temperature.

The molecular-dynamics results show that the FSDP is between 1.3 and 1.4 Å^{-1} both in the molten and amorphous states. The experimental value for the peak position is 1 Å^{-1}. Uemura *et al.*[1] have observed that the height of the first peak is slightly larger in the molten state than in the glass. Susman *et al.*[3] find that the height of the FSDP is about the same in the molten and

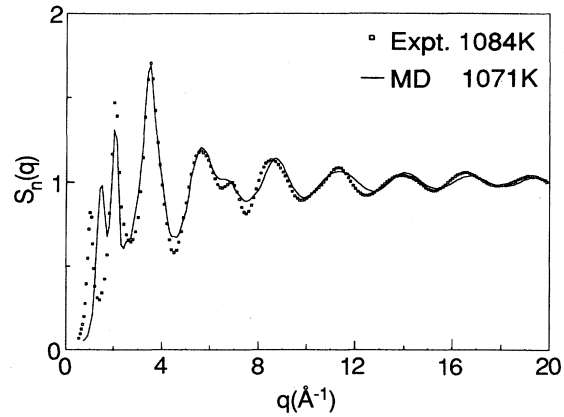

FIG. 13. Neutron-scattering static-structure factor in a-$GeSe_2$. Solid line, MD result at $T=283$ K; open squares, experimental neutron-diffraction results at $T=10$ K, Susman *et al.* (Ref. 15).

glassy states at 1084 and 10 K, respectively.

Let us investigate the correlations that give rise to the first peak. It has been suggested that the FSDP in $GeSe_2$ is due to layerlike correlations[21] and that the inverse interlayer separation corresponds to the observed peak position in the q space. Another explanation is that the peak arises from the random packing of $Ge(Se_4)_{1/2}$ tetrahedra.[5] From partial static-structure factors in Figs. 10 and 11, it is clear that Se-Se correlations do not contribute to the FSDP, but Ge-Se and Ge-Ge do since both $S_{Ge\text{-}Ge}(q)$ and $S_{Ge\text{-}Se}(q)$ have peaks at $q \approx 1.4$ Å^{-1}. To ascertain the role of Ge correlations further, we performed a calculation in which the partial pair-distribution functions were cutoff at 8.8 Å instead of the usual[46] 18.8 Å. The partial structure factors resulting from this are shown in Fig. 14. The first peak at 1.4 Å^{-1} disappears in $S_{Ge\text{-}Ge}(q)$ but not in $S_{Ge\text{-}Se}(q)$ and Fig. 15 shows the near disappearance of the FSDP in the total static structure factor. This strongly suggests that Ge-Ge correlations are largely responsible for this peak. Experiments on $GeTe_2$-$GeSe_2$ series reveal that the FSDP grows considerably as Te is replaced by the weaker scattering Se atoms so as to enhance the Ge contribution.[47] Fuoss *et al.*[35] arrived at the same conclusion through differential-anomalous-scattering experiments. The FSDP is considerably larger near the Ge edge than near the Se edge.

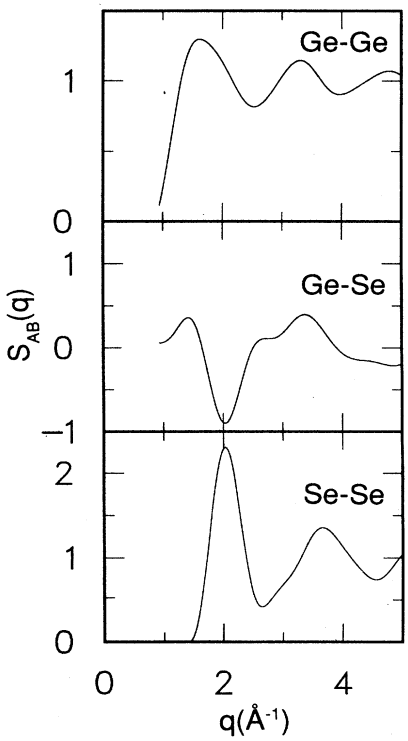

FIG. 14. Partial static-structure factors in a-$GeSe_2$ obtained from the Fourier transforms of truncated partial pair-distribution functions. The truncation removes any spatial correlations beyond 8.8 Å. Note that the first peak around 1.4 Å^{-1} in $S_{Ge\text{-}Ge}(q)$ disappears whereas the peak in $S_{Ge\text{-}Se}(q)$ is unaffected by the truncation of spatial correlations. See discussion of the structure factor in Sec. IV.

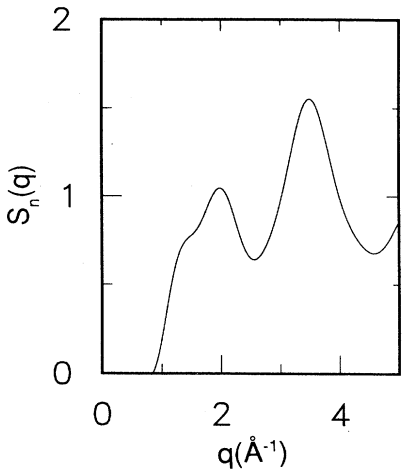

FIG. 15. Neutron-scattering static-structure factor for a-$GeSe_2$ with spatial correlations truncated at 8.8 Å. Comparing this with Fig. 13, one observes the disappearance of the first sharp diffraction peak at $q = 1.4$ Å^{-1} as result of truncation.

Having determined that Ge-Ge and to a lesser extent Ge-Se correlations are responsible for the FSDP, let us investigate the range of spatial correlations that give rise to this peak. Figures 16 and 17 show the pair-distribution function and the static-structure factor for Ge-Ge in the glass (283 K) and molten states at 1071 and

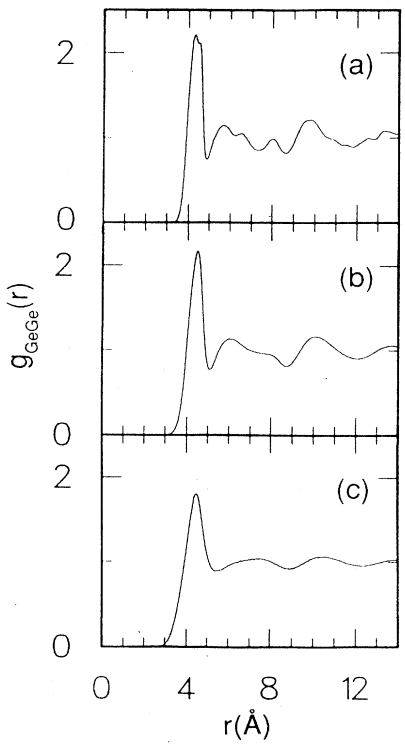

FIG. 16. Pair-distribution function for Ge-Ge in (a) the vitreous state at $T = 283$ K and $\rho = 3.443 \times 10^{22}$ cm^{-3}, and molten states at (b) $T = 1071$ K and (c) $T = 2055$ K. The number density in the molten state is 3.114×10^{22} cm^{-3}.

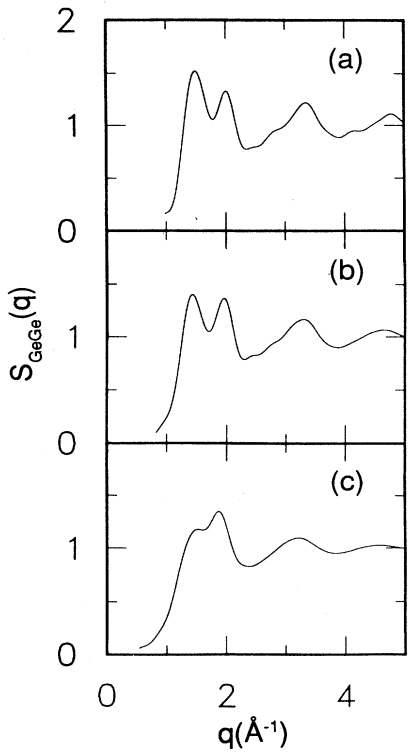

FIG. 17. (a) Static-structure factor for Ge-Ge in the vitreous state at $T=283$ K and $\rho=3.443\times10^{22}$ cm^{-3}. $S_{\text{Ge-Ge}}(q)$ for molten states ($\rho=3.114\times10^{22}$ cm^{-3}) at $T=1071$ and 2055 K are shown in (b) and (c), respectively.

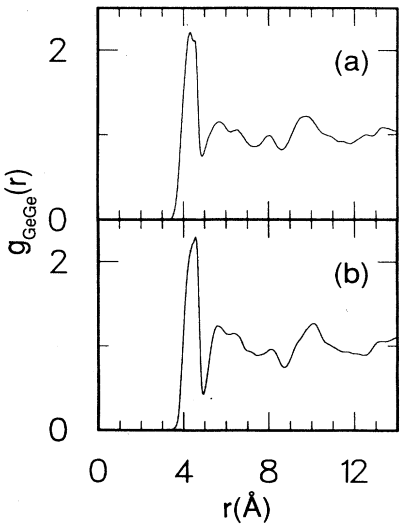

FIG. 18. Ge-Ge pair-distribution function in a-$GeSe_2$ at (a) $\rho=3.443\times10^{22}$ cm^{-3} and (b) $\rho=3.114\times10^{22}$ cm^{-3}. The temperature of both systems is around 300 K.

2055 K. Recall that the FSDP almost disappears when the correlations are terminated at 8.8 Å, thereby excluding the peak at 10 Å. Thus, Ge-Ge correlations in the range of 10 Å and Ge-Se correlations in the range of 6 Å are responsible for the first sharp diffraction peak.

Finally, let us examine the anomalous temperature dependence of the FSDP. We have found that the height of the FSDP is slightly greater in the molten state at 1071 K than in the glass at 283 K, see Figs. 12 and 13. Neutron-scattering results[3] in Figs. 12 and 13 indicate that the height of the FSDP is approximately the same in the molten and vitreous states. However, Uemura *et al.*[1] have observed the anomalous temperature dependence of the FSDP just as in our MD results. We will now demonstrate that the anomalous temperature dependence is due to an increase in the density of the system when quenched from the molten to the glass state. Figures 16(b) and (16c) display the pair-distribution functions for Ge-Ge when the molten state is cooled from 2000 to 1100 K keeping the density fixed at 3.114×10^{22} cm^{-3}. All the peaks broaden as a result of heating. We performed a simulation in which the molten state at 1100 K is quenched to 300 K keeping the density fixed at 3.114×10^{22} cm^{-3}. The results for $g_{\text{Ge-Ge}}(r)$ are displayed in Fig. 18(b) whereas $S_{\text{Ge-Ge}}(q)$ are shown in Fig. 19(b). Clearly the peaks in $g_{\text{Ge-Ge}}(r)$ are sharper in the glass at 300 K because of thermal narrowing. We then increased the density of the glass to 3.443×10^{22} cm^{-3}, thermalized the system at 283 K for 15 000 time steps, and ran it for an additional 36 000 time steps. Figures 18 and 19 show Ge-Ge pair-distribution functions and static-structure factors, respectively, of the glass at the two densities. It is clear that the peaks in $g_{\text{Ge-Ge}}(r)$ and $S_{\text{Ge-Ge}}(q)$ broaden and also shift slightly due to the increase in the density of the amorphous state. Concommitantly, the height of the FSDP decreases as shown in Fig. 20. An increase in the density of a disordered system increases the frustration which, in turn, broadens the peaks in the pair-distribution functions and lowers the height of the FSDP. As we have discussed earlier in Sec.

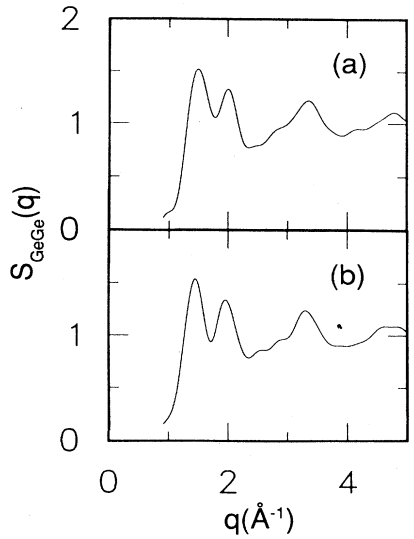

FIG. 19. Ge-Ge static-structure factor in a-$GeSe_2$ at (a) $\rho=3.443\times10^{22}$ cm^{-3} and (b) $\rho=3.114\times10^{22}$ cm^{-3}. The temperature of both systems is around 300 K.

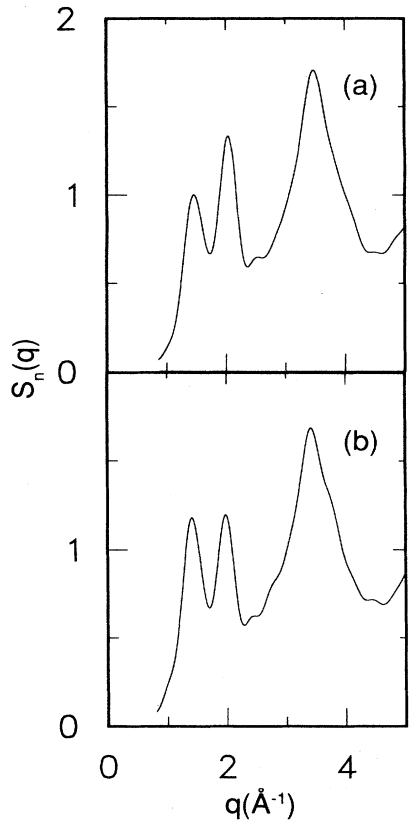

FIG. 20. MD results for the neutron-scattering static-structure factor in a-$GeSe_2$ at $T\sim 300$ K. (a) $\rho=3.443\times10^{22}$ cm^{-3} and (b) $\rho=3.114\times10^{22}$ cm^{-3}.

IV C, the FSDP is mainly due to Ge-Ge correlations in the range of 10 Å and Ge-Se correlations in the range of 6 Å. When the density of the system is increased, the weaker medium-range correlations are more easily affected. This is why the FSDP and not the other peaks in the static-structure factor exhibit the anomalous variation with temperature.

Using the same functional form for the model potential [Eq. (1)] but with parameters appropriate for SiO_2, we have MD results indicating that the FSDP in a-SiO_2 occurs at $q=1.5$ Å^{-1}. This is again in good agreement with experiments. The presence of this peak in both SiO_2 and $GeSe_2$ gives credence to the model potential for AX_2-type glasses.

B. Phonon density of states

Walter *et al.*[15] have recently measured an effective density of states (DOS) in a-$GeSe_2$ using inelastic-neutron-scattering technique. The measurements reveal five prominent peaks at 9, 11, 25.7, 33, and 36.5 meV. In addition, there are weaker features at 18.5 and 39 meV. The Raman-scattering data[21] reveal Raman-active lines at 10, 17, 22, 25, 26.5, 32, and 38 meV. The 25-meV line arises from the symmetric breathing mode A_1 and the 26.5 meV is the well-known companion line of A_1. A great deal of experimental work[16,17,21] deals with A_1 and its companion line, A_{1c}. It has been suggested that this line is due to layerlike structure in the glass.[21]

There are two ways to obtain the phonon density of states by the MD technique. At low temperature[48,49] the frequency spectrum of the normalized velocity autocorrelation function $Z(t)$ relates to density of states $G(\omega)$,

$$G(\omega)=\frac{6N}{\pi}\int_0^{\tau}Z(t)\cos(\omega t)e^{-\lambda(t/\tau)^2}dt\ , \tag{6}$$

where

$$Z_\alpha(t)=\frac{\left\langle\sum_i \mathbf{V}_{i\alpha}(t)\cdot\mathbf{V}_{i\alpha}(0)\right\rangle}{\left\langle\sum_i \mathbf{V}_{i\alpha}^2(0)\right\rangle}\ , \tag{7a}$$

$$Z(t)=\sum_\alpha C_\alpha Z_\alpha(t)\ . \tag{7b}$$

In the Gaussian representing a window function, we have chosen $\lambda=1$ and $\tau=3ps$. The large brackets $\langle\ \rangle$ in Eq. (7) denote the ensemble average.

Beeman and Alben[50] have proposed an alternative method for calculating various spectra for linear harmonic problems without having to diagonalize the dynamical matrix In this so-called equations of motion approach, the displacements from equilibrium are integrated forward in time and the density of states is calculated from

$$G(\omega)=\frac{4}{\pi\delta_m^2}\int_0^{\tau}f(t)\cos(\omega t)e^{-\lambda(t/\tau)^2}dt\ , \tag{8}$$

where

$$f(t)=\sum_{i\alpha}\delta x_{i\alpha}(t)\delta x_{i\alpha}(0)\ , \tag{9}$$

and

$$\delta x_{i\alpha}(t)=x_{i\alpha}(t)-x_{i\alpha 0}\ . \tag{10}$$

The equilibrium positions $x_{i\alpha 0}$ of the atoms are obtained by applying the steepest-descent method[44] to an MD configuration, thereby locating the underlying local minimum where the velocity and the force on each particle is zero. The time variation of $x_{i\alpha}(t)$ is calculated by integrating the Newtonian equations of motion as in an MD calculation.

Beeman and Alben suggest the following prescription for initial displacements:

$$\delta x_{i\alpha}(0)=\delta_m\cos\theta_{i\alpha}\ , \tag{11}$$

where i $(=1,2,\ldots,N)$ and α denote a particle and its Cartesian components, respectively, and $\theta_{i\alpha}$ are random angles distributed uniformly between 0 and 2π. We choose the amplitude of the initial displacement, δ_m, to be equal to 0.04 Å and we perform averages over $G(\omega)$'s with different sets of $\theta_{i\alpha}$'s to improve the accuracy of the calculation.

Figures 21 and 22 show the frequency spectra of velocity autocorrelation functions for Ge and Se in the molten and vitreous states, respectively. In Fig. 23(a) we show the total density of states in the glass ($T=283$ K) and, for comparison, the frequency spectrum of the velocity autocorrelation function in the molten state is shown in

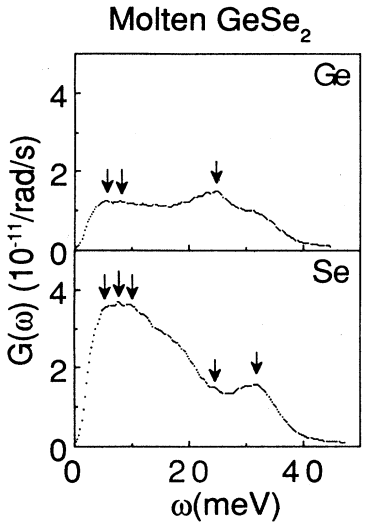

FIG. 21. Fourier transforms of velocity autocorrelation functions [Eqs. (6) and (7)] of Ge and Se in the molten state at 1071 K.

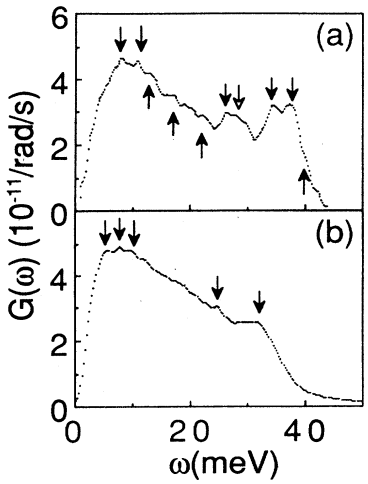

FIG. 23. Total density of states in (a) vitreous and (b) molten $GeSe_2$. The density of states in the molten phase is calculated from Eqs. (6) and (7), and in the vitreous state from Eqs. (8)–(11).

Fig. 23(b). The main peaks in the MD density of states [Fig. 23(a)] occur at 8.0, 10.8, 26.4, 34.4, and 37.2 meV. These results are in good agreement with the inelastic-neutron-scattering measurements,[15] see Fig. 24, where the prominent peaks are observed at 9, 11, 25.7, 33, and 36.5 meV.

It is commonly believed that four of these peaks are associated with the internal modes of an isolated $Ge(Se_{1/2})_4$ tetrahedron. Since these tetrahedra remain intact in the molten state, the internal modes could be ascertained by comparing the frequency spectra of the velocity autocorrelation function in molten $GeSe_2$ with the phonon density-of-states in a-$GeSe_2$. Figure 23 shows that the 8.0- and 10.8-meV peaks in a-$GeSe_2$ merge into a single peak around 10 meV while the peaks at 26.4 and 34.4 meV remain distinct in the molten state.

Sen and Thorpe[34] have argued that the normal-mode description of an isolated tetrahedron in an AB_2-type system is valid when the A—B—A bond angle is around 90°. In that case, it suggested that the system consists of weakly interacting tetrahedral units. On the other hand, if the A—B—A bond angle is close to 180°, there is a great deal of overlap between neighboring tetrahedra and the phonon spectrum consists of bandlike modes. The value of the A—B—A angle delineating this transition is given by $\theta_c = \cos^{-1}(-2M_B/3M_A)$. For $GeSe_2$, $\theta_c = 136°$. The Ge—Se—Ge bond-angle distribution in Fig. 7 has a broad peak (at 125°) close to θ_c and therefore considerable modification of molecular $Ge(Se_{1/2})_4$ modes is expected.

The MD results for density of states indicate a feature (27.8 meV) close to the A_1 line at 26.4 meV. In Raman-scattering measurements a companion of the A_1 mode is observed at approximately 1.8 meV higher than the ener-

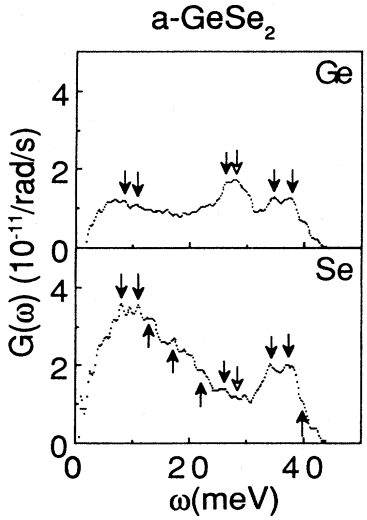

FIG. 22. Partial density of states of Ge and Se in a-$GeSe_2$. The density of states are calculated from the Fourier transforms of position-position correlation functions [Eqs. (8)–(11)].

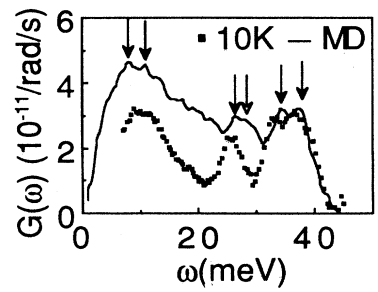

FIG. 24. Calculated total phonon density of states for a-$GeSe_2$ at $T=0$ K obtained from Eqs. (8)–(11) compared with the neutron density of states at 10 K.

gy of the A_1 mode. The well-known companion line A_{1c} has been thoroughly investigated in the crystalline and amorphous states[16–18,21] by Raman scattering. In c-$GeSe_2$,[21] the two lines are at 210.3 cm^{-1} (26.1 meV) and 215.3 cm^{-1} (26.7 meV) whereas in the glass they are observed at 198 cm^{-1} (24.5 meV) and 212 cm^{-1} (26.3 meV). There are conflicting points of view on the origin of the companion line. It has been attributed to vibrations in (i) fivefold, sixfold, and sevenfold rings,[17] (ii) edge-sharing tetrehedra,[45] and (iii) Se dimers in an outrigger-raft model.[21]

To identity the source of the companion line, we have calculated the density of states of a tetrahedron belonging to different sizes of rings. There is no signature of the companion peak in twofold (edge-sharing) or threefold rings. The breathing mode (A_1) and the companion line A_{1c} are well resolved for tetrahedra belonging to five and sevenfold rings but *not* in sixfold rings.

In the phonon density of states we also find weaker peaks around 12.6, 17.2, 22.0 meV, and a shoulder around 40 meV. The inelastic-neutron-scattering measurements[15] indicate a small peak at 18 meV and Raman-active lines have been observed[21] at 17 and 22 meV. In both neutron- and Raman-scattering studies there are indications of a phonon feature around 39 meV.

V. CRITIQUE

Molecular-dynamics calculations based on the effective potential in Eq. (1) provide considerable insight into microscopic processes in molten and glassy $GeSe_2$. The MD results display all the peaks observed in the neutron- and x-ray-diffraction measurements. The peak positions and their relative heights are in good agreement with experiments. The MD calculations can also explain the origin and the anomalous temperature variation of the first sharp diffraction peak. The FSDP is found to be due to Ge-Ge and Ge-Se correlations, which is in agreement with differential anomalous x-ray-scattering experiments. The observed decrease in the height of the FSDP on cooling is directly attributable to enhanced frustration resulting from an increase in the number density.

Insofar as the structural results are concerned, the only discrepancy is in the position of the FSDP: the peak is between 1.3 and 1.4 $Å^{-1}$ in the MD calculations, whereas experimentally it is observed between 1.0–1.1 $Å^{-1}$. We feel that three-body forces will alter the range of medium-range correlations and the FSDP will therefore shift to a lower wave vector. This is supported by preliminary molecular-dynamics calculations which include three-body interactions.

The results for phonon density of states are also in good agreement with neutron- and Raman-scattering measurements. We have observed a feature close to the peak corresponding to the symmetric breathing mode. The energy of the companion feature is 1.5 meV higher than that of the breathing mode which is in good agreement with Raman-scattering measurements.

The success of MD calculations in $GeSe_2$ paves the way for investigating the structural and dynamical correlations in other binary chalcogenide glasses using similar effective interparticle potentials. These MD calculations are now in progress.

ACKNOWLEDGMENTS

We would like to thank our colleagues Dr. D. L. Price and Dr. S. Susman for many stimulating discussions, valuable advice, and for providing us with a wealth of unpublished neutron-scattering results. We also acknowledge many fruitful conversations with Dr. G. A. Antonio, Dr. M. Grimsditch, Dr. L. Guttman, Dr. D. Koelling, Dr. A. Wright, Dr. J. P. Rino, Dr. H. Iyetomi, and Dr. D. Montague. One of us (P.V.) would like to acknowledge the kind hospitality of the Laboratory of Atomic and Solid State Physics and the Center for Theory and Simulation in Science and Engineering, Cornell University, and another (I.E.) would like to thank the Swedish Research Council and Argonne National Laboratory for their support. This work was supported in part by the Office of Energy Research Cray Research X-MP 48 computer at the National Magnetic Fusion Energy Computing Center (Livermore, CA). This work was supported by the U.S. Department of Energy (Division of Materials Sciences of the Office of Basic Energy Sciences, under Contract No. W-31-109-ENG-38.

*Permanent address.

[1]O. Uemura, Y. Sagara, and T. Satow, Phys. Status Solidi A **32**, K91 (1975); O. Uemura, Y. Sagara, D. Muno, and T. Satow, J. Non-Cryst. Solids **30**, 155 (1978).

[2]R. J. Nemanich, F. L. Galeener, J. C. Mikkelsen, G. A. N. Connell, G. Etherington, A. C. Wright, and R. N. Sinclair, Physica B+C **117&118B**, 959 (1983).

[3]S. Susman, D. G. Montague, D. L. Price, and K. G. Volin (unpublished).

[4]A. Feltz, M. Pohle, H. Steile, and G. Helms, J. Non-Cryst. Solids **69**, 271 (1985).

[5]S. C. Moss and D. L. Price, in *Physics of Disordered Materials*, edited by D. Adler, H. Fritzsche, and S. R. Ovshinsky (Plenum, New York, 1985), p. 77.

[6]A. C. Wright, R. N. Sinclair, and A. J. Leadbetter, J. Non-Cryst. Solids **71**, 295 (1985).

[7]J. C. Phillips, J. Non-Cryst. Solids **43**, 37 (1981).

[8]L. E. Busse and S. R. Nagel, Phys. Rev. Lett. **47**, 1848 (1981); L. E. Busse, Phys. Rev. B **29**, 3639 (1981).

[9]A. I. Soklakov and V. V. Nechaeva, Fiz. Tverd. Tela (Leningrad) **9**, 921 (1967) [Sov. Phys.—Solid State **9**, 715 (1967)].

[10]M. Misawa and N. Watanabe, Tsukuba National Laboratory for High Energy Physics, Japan, Report No. KENS-IV, 1983 (unpublished).

[11]C. Lin, L. E. Busse, S. R. Nagel, and J. Faber, Phys. Rev. B **29**, 5060 (1984).

[12]R. W. Johnson, D. L. Price, S. Susman, T. I. Morrison, and G. K. Shenoy, J. Non-Cryst. Solids **83**, 251 (1986).

[13]M. F. Daniel, A. J. Leadbetter, A. C. Wright, and R. N. Sinclair, J. Non-Cryst. Solids **32**, 271 (1979).
[14]D. L. Price, M. Misawa, S. Susman, T. I. Morrison, G. K. Shenoy, and M. Grimsditch, J. Non-Cryst. Solids **66**, 443 (1984).
[15]U. Walter, D. L. Price, S. Susman, and K. J. Volin, Phys. Rev. B **37**, 4232 (1988).
[16]P. Tronc, M. Bensoussan, A. Brenac, and C. Sebenne, Phys. Rev. B **8**, 5947 (1973).
[17]R. J. Nemanich, S. A. Solin, and G. Lucovsky, Solid State Commun. **21**, 273 (1977).
[18]N. Kumagai, J. Shirafuji, and Y. Inuishi, J. Phys. Soc. Jpn. **42**, 1262 (1977).
[19]R. J. Nemanich, G. A. N. Connell, T. M. Hayes, and R. A. Street, Phys. Rev. B **18**, 6900 (1978).
[20]H. Kawamura and M. Matsumura, Solid State Commun. **32**, 83 (1979).
[21]P. M. Bridenbaugh, G. P. Espinosa, J. E. Griffiths, J. C. Phillips, and J. P. Remeika, Phys. Rev. B **20**, 4140 (1979).
[22]H. Kawamura, M. Matsumura, and S. Ushioda, J. Non-Cryst. Solids **35&36**, 1215 (1980).
[23]J. E. Griffiths, G. P. Espinosa, J. P. Remeika, and J. C. Phillips, Solid State Commun. **40**, 1077 (1981).
[24]J. E. Griffiths, G. P. Espinosa, J. P. Remeika, and J. C. Phillips, Phys. Rev. B **25**, 1272 (1982).
[25]J. E. Griffiths, J. C. Phillips, G. P. Espinosa, and J. P. Remeika, Phys. Rev. B **26**, 3499 (1982).
[26]T. Fukunaga, Y. Tanaka, and K. Murase, Solid State Commun. **42**, 513 (1982).
[27]J. E. Griffiths, G. P. Espinosa, J. C. Phillips, and J. P. Remeika, Phys. Rev. B **28**, 4444 (1983).
[28]M. Balkanski, E. Haro, G. P. Espinosa, and J. C. Phillips, Solid State Commun. **51**, 639 (1984).
[29]M. Stevens, P. Boolchand, and J. G. Hernandez, Phys. Rev. B **31**, 981 (1985).
[30]E. Haro, Z. S. Xu, J.-F. Morhange, M. Balkanski, G. P. Espinosa, and J. C. Phillips, Phys. Rev. B **32**, 969 (1985).
[31]J. E. Griffiths, J. C. Phillips, G. P. Espinosa, J. P. Remeika, and P. M. Bridenbaugh, Phys. Status Solidi B **122**, K11 (1984).
[32]K. Murase, T. Fukunaga, Y. Tanaka, K. Yakushiji, and I. Yunoki, Physica B+C **117&118B**, 962 (1983).
[33]G. Lukovsky, C. K. Wong, and W. B. Pollard, J. Non-Cryst. Solids **59&60**, 839 (1983).
[34]P. N. Sen and M. F. Thorpe, Phys. Rev. B **15**, 4030 (1977).
[35]P. H. Fuoss, P. Eisenberger, W. K. Warburton, and A. Bienenstock, Phys. Rev. Lett. **46**, 1537 (1981).
[36]P. Vashishta, Solid State Ionics **18&19**, 3 (1986); P. Vashishta and A. Rahman, Phys. Rev. Lett. **40**, 1337 (1978); P. Vashishta and A. Rahman, *Fast Ion Transport in Solids,* edited by P. Vashishta, J. N. Mundy, and G. K. Shenoy (Elsevier, New York, 1979), p. 527; P. Vashishta, I. Ebbsjö, R. Dejus, and K. Sköld, J. Phys. C **18**, L291 (1985); I. Ebbsjö, P. Vashishta, R. Dejus, and K. Sköld, *ibid.* **20**, L441 (1987).
[37]A. Rahman and P. Vashishta, in *The Physics of Superionic Conductors,* edited by J. W. Perram (Plenum, New York, 1983), p. 93; M. Parrinello, A. Rahman, and P. Vashishta, Phys. Rev. Lett. **50**, 1073 (1983); J. Ray, A. Rahman, and P. Vashishta, in *Superionic Solids,* edited by A. Laskar and S. Chandra (Academic, New York, 1987).
[38]P. Vashishta, I. Ebbsjö, and R. K. Kalia, Bull. Am. Phys. Soc. **30**, 236 (1985).
[39]C. Kittel, *Introduction to Solid State Physics* (Wiley, New York, 1971).
[40]H. Ipser, M. Gambino, and W. Schuster, Monatshefte für Chemie **113**, 389 (1982).
[41]S. Susman (private communication).
[42]D. Beeman, J. Comp. Phys. **20**, 130 (1976).
[43]F. H. Stillinger and T. A. Weber, Science **225**, 983 (1984).
[44]Von G. Dittmar and H. Schäfer, Acta Crystallogr. Sect. B **37**, 2726 (1976).
[45]S. Sugai, Phys. Rev. B **35**, 1345 (1987).
[46]The pair-distribution functions are calculated up to $(L/2)\sqrt{2}$ with a reduced spherical shell between $L/2$ and $(L/2)\sqrt{2}$.
[47]S. C. Moss, in *Proceedings of the Fifth International Conference on Amorphous and Liquid Semiconductors* (Taylor and Francis, London, 1974), p. 17.
[48]An n-fold ring is determined as follows: Starting with a Ge atom in a given configuration, we locate the positions of the rest of the atoms in the MD cell around the central Ge atom. Next the nearest-neighbor Se atoms of the central Ge atom are determined in a sphere of radius 3.1 Å—the distance at which the first peak in $g_{\mathrm{Ge\text{-}Se}}(r)$ terminates. Moving to one of the Se atoms, we determine its nearest-neighbor Ge atoms excluding the previous Ge atom. This procedure is continued until one of the atoms in the $(n+1)$th sequence is the central Ge atom. This defines an n-fold ring containing n Ge and an equal number of Se atoms.
[49]P. A. V. Johnson, A. C. Wright, and R. N. Sinclair, J. Non-Cryst. Solids **58**, 109 (1983).
[50]D. Beeman and R. Alben, Adv. Phys. **26**, 339 (1977).